Measurement of quantum memory effects and its fundamental limitations

Matthias Wittemer,[*] Govinda Clos, Heinz-Peter Breuer, Ulrich Warring, and Tobias Schaetz

Physikalisches Institut, Universität Freiburg, Hermann-Herder-Straße 3, D-79104 Freiburg, Germany

We discuss that the nature of projective measurements in quantum mechanics can lead to a nontrivial bias in non-Markovianity measures, quantifying the flow of information between a system and its environment. Consequently, in the current form, envisioned applications are fundamentally limited. In our trapped-ion system, we precisely quantify such bias and perform local quantum probing to demonstrate corresponding limitations. The combination of extended measures and our scalable experimental approach can provide a versatile reference, relevant for understanding more complex systems.

In nature any quantum system inevitably interacts with its environment [1]. This interaction induces dynamics, which creates classical and quantum correlations, and will eventually lead to decoherence and dissipation for observables of the *open* system. Common approaches to enable a description of the open system dynamics involve the approximation of a Markovian process, i.e., a memoryless time evolution. However, in many cases this assumption is not justified, and distinct dynamical features witness underlying non-Markovian behavior.

The classical definition of non-Markovianity (NM) fails in the quantum regime due to the special role of measurements as described by the projection postulate [2]. Recently, several definitions of quantum NM as well as quantitative measures have been developed [3–8], see reviews [2,9,10]. The physical implications of memory effects initiate a variety of applications for diverse quantum systems and phenomena, e.g., Ising or Heisenberg spin chains and Bose-Einstein condensates [11–13], optomechanical systems [14], chaotic systems [15,16], quantum dots [17], energy-transfer processes in photosynthetic complexes [18], and quantum metrology [19]. In particular, quantum memory measures are discussed to enable local probing of otherwise inaccessible characteristics of physical systems, e.g., in the context of Anderson localization [20] and quantum phase transitions [13,21].

The definition of quantum NM developed in Ref. [4] features a physical interpretation based on concepts of quantum information theory. It employs a distance measure in state space to characterize the distinguishability of quantum states [22] of the open system. In this context, NM is identified as a backflow of information to the system, i.e., as an increase in distinguishability. So far, NM and related initial system-environment correlations have been experimentally observed in photonic [23–29], nuclear magnetic resonance [30], and trapped-ion systems [31].

Trapped atomic ions are well suited to further investigate aspects of memory effects. Individual control of electronic and motional degrees of freedom permit the realization of effective spins with tunable couplings via or to bosonic degrees of freedom [32–37]. Techniques for preparation, (coherent) manipulation, effective interaction, and detection of quantum states are performed with efficiencies close to unity [33,34,38–40]. Isolation from surroundings approximates a closed system with parameters that can be tuned continuously—from a simple toylike system, still allowing for exact numerical treatment of pure and mixed states, up to complex system-environment configurations and interactions [35–37,41–44].

In this Rapid Communication, we study fundamental aspects of quantum NM in a trapped-ion system and challenge current understandings of non-Markovian system-environment interactions by approaching from a most simple showcase. We precisely quantify the exchange of information between an open system and its well-defined quantum environment with the measure defined in Ref. [4]. Thereby, we reveal that the nature of projective measurements in quantum mechanics can fundamentally limit envisioned applications. We demonstrate a local quantum probing application to highlight this phenomenon. We thereby suggest that our system can be used as a versatile reference for further studies.

To define quantum NM for a system S interacting with its environment E, the authors of Ref. [4] suggest utilizing the time evolution of the trace distance $D(t) \equiv \frac{1}{2}\|\rho_S^1(t) - \rho_S^2(t)\|$. It quantifies the distinguishability of two system states $\rho_S^{1,2}$ [22], which are obtained by tracing out the environmental degrees of freedom. While Markovian processes are defined by a monotonic decrease in $D(t)$, the characteristic feature of non-Markovian dynamics is any increase in $D(t)$ [4]. The accumulated growth of D within a maximal duration $t_{\max}$, where D is sampled in steps of Δt, is quantified by [4]

$$\mathcal{N} = \sum_{t=\Delta t}^{t_{\max}} [D(t) - D(t - \Delta t)]_{>0}. \qquad (1)$$

Explicitly, the sum extends over all positive changes in $D(t)$. In the following, we consider the NM corresponding to a representative pair of orthogonal initial states $\rho_S^{1,2}(t = 0)$. We note that the choice of the sampling rate $\gamma \equiv 1/\Delta t$ and $1/t_{\max}$ defines the highest and lowest frequencies, respectively, with which a growth in D can be detected.

*Corresponding author: matthias.wittemer@physik.uni-freiburg.de

In classical probability theory, there exists a mathematical condition for stochastic processes to be Markovian in terms of conditional probability distributions [45]. This definition cannot be transferred to the quantum regime as quantum states change discontinuously and randomly conditioned on the outcomes of projective measurements. In particular, measurements on the open system completely destroy all—classical and quantum—correlations between system and environment. Hence, they strongly influence the subsequent dynamics [2]. On one hand, Eq. (1) provides a clear definition for a measure of quantum NM which is independent of measurement-induced state changes described by the projection postulate. On the other hand, measurements are subjected to intrinsic uncertainties, referred to as *quantum projection noise* (QPN) [46]: Consider a superposition state of a two-level system $|\psi\rangle \equiv c_A |A\rangle + c_B |B\rangle$ with $|c_A|^2 + |c_B|^2 = 1$. Any projective measurement transfers $|\psi\rangle$ into the pointer basis of the measurement device. For example, if the pointer basis is $\{|A\rangle, |B\rangle\}$, the result indicates either $|A\rangle$ or $|B\rangle$ with probability $|c_A|^2$ or $|c_B|^2$, respectively. Consequently, expectation values can only be determined by averaging r repetitions. The related statistical uncertainty is proportional to $1/\sqrt{r}$ and persists, even in the absence of any uncertainty in state preparation. We point out that the mathematical definition of $\mathcal{N}$ translates the QPN into a systematic bias $\mathcal{B}$. This yields the explicit functional dependence $\mathcal{N} = \mathcal{N}(t_{\max}, \gamma, r)$. We regard values with zero QPN and infinite γ as *true* values, i.e., $\mathcal{N}_{\text{true}} \equiv \lim_{\gamma, r \to \infty} \mathcal{N}(t_{\max}, \gamma, r)$. We identify $\mathcal{B} \equiv \mathcal{N} - \mathcal{N}_{\text{true}}$ to be a nontrivial function of the particular evolution $D(t)$ and the parameters $t_{\max}$, γ, and r. In addition, any kind of noise, including technical or numerical imperfections, contributes to an excess bias, as remarked in Ref. [16]. Contrary to common intuition, the overall bias can continue to increase and lead to less accurate values of $\mathcal{N}$ when increasing measurement efforts.

In order to investigate properties of non-Markovian quantum dynamics, we consider the following toy system. It is composed of a single spin-1/2, representing the open system S, and a bosonic degree of freedom that spans its environment E, see Fig. 1. The bipartite system $S + E$ is assumed to be isolated from an additional surrounding X. We write the open system's Hamiltonian as $H_S = \hbar \omega_z \sigma_z / 2$, where σ_z is the Pauli matrix with eigenstates $|\downarrow\rangle$ and $|\uparrow\rangle$ and effective energy splitting $\hbar \omega_z$ and the reduced Planck constant $\hbar$. The environment is represented by the Hamiltonian $H_E = \hbar \omega_E a^\dagger a$ with annihilation (creation) operators a $(a^\dagger)$ and eigenfrequency ω_E, and the Fock states are labeled n. The dynamics of the total system $S + E$ is governed by the Hamiltonian [35],

$$H = H_S + H_E + H_I$$
$$= \frac{\hbar \omega_z}{2} \sigma_z + \hbar \omega_E a^\dagger a + \frac{\hbar \Omega}{2} [\sigma^+ e^{i\eta(a^\dagger + a)} + \text{H.c.}]. \quad (2)$$

Here, we express the interaction term H_I by the spin coupling rate Ω, spin-flip operators $\sigma^\pm \equiv (\sigma_x \pm i \sigma_y)/2$, Pauli matrices $\sigma_{x,y}$, and the spin-boson coupling-parameter η. We investigate the evolution of initial product states $\rho(0) = \rho_S(0) \otimes \rho_E(0)$ with two representative states $\rho_S^1(0) \equiv |\uparrow\rangle \langle\uparrow|$ and $\rho_S^2(0) \equiv |\downarrow\rangle \langle\downarrow|$ and thermal states $\rho_E(0)$ defined by average occupation numbers $\bar{n}$. We choose $\rho_E(0)$ near the ground state to
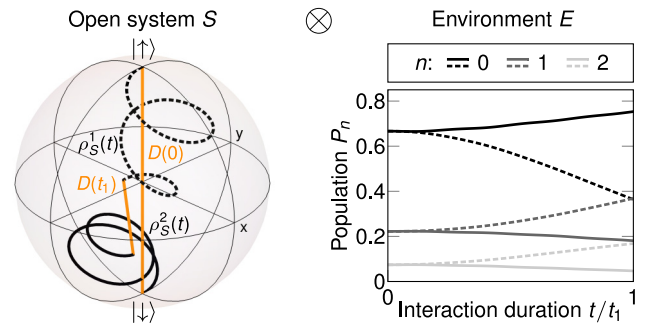

FIG. 1. Toy system to study quantum memory effects. Illustration of the total system, composed of a single spin-1/2, initially in $\rho_S^1(0) = |\uparrow\rangle \langle\uparrow|$ (the dashed lines) or $\rho_S^2(0) = |\downarrow\rangle \langle\downarrow|$ (the solid lines), and a bosonic environment, initially in a thermal state with low $\bar{n}$. (Left) $\rho_S^{1,2}(t)$ in the Bloch-sphere representation and (right) related populations of the $n = \{0\text{--}2\}$ environmental states. Information is transferred from S to E and into correlations or entanglement (not depicted); the amount is accounted for by the change of distinguishability $D(t)$ of $\rho_S^{1,2}(t)$.

ensure that energies of spin and bosonic degrees of freedom remain comparable, enabling observations of distinct features of quantum memory. In Fig. 1, we illustrate an exemplary time evolution $\rho_S^{1,2}(t)$ and changes in Fock-state populations that indicate a transfer of information from S to E.

In our experiment, we implement H with a single trapped $^{25}\text{Mg}^+$. For all measurements, we ensure that residual decoherence rates Γ_{dec} due to couplings to X (technical noise) are negligible $\Gamma_{\text{dec}} \ll 1/t_{\max} < \Omega$ (see the Supplemental Material [47]). Two electronic hyperfine states form S, whereas E is composed of a motional mode with frequency $\omega_E/(2\pi) = 1.920(3)$ MHz. The coherent S-E interaction H_I is implemented via two-photon stimulated Raman transitions [33] with $\Omega/(2\pi) \approx 100$ kHz and $\eta \approx 0.32$. More details on implementation and analysis are described in [47] and Refs. [36,37]. To record $D(t)$, we perform a measurement series of time-resolved spin-state tomography [33]. Each sequence starts with the initialization of $\rho_S^1(0)$ or $\rho_S^2(0)$ with dedicated $\bar{n}$. We implement H for variable duration $t \in [0, 9\tau]$ with $\tau \equiv 2\pi/\Omega$. Subsequently, we detect expectation values $\langle \sigma_l(t) \rangle$ $(l = x, y, z)$ in individual sequences for each l with fixed $r = r_0 \equiv 500$ and $\gamma = \gamma_0 \approx 15\tau^{-1}$. From the recorded $\langle \sigma_l(t) \rangle$, we determine $\rho_S^{1,2}(t)$, the corresponding $D(t)$ and $\mathcal{N}$, and their statistical uncertainties [47]. To assess systematic effects of our measurements, we compare our data with numerical simulations of the total system dynamics generated by H, see Refs. [37] and [47]. We conduct independent calibration measurements to determine corresponding parameters ω_E, ω_z, Ω, and $\bar{n}$. In particular, we choose γ and r according to our experimental realizations to generate numerically simulated values for the averages $\langle \sigma_l \rangle_{\text{sim}}$. These yield the dispersion of D_{sim} and values $\mathcal{N}_{\text{sim}}$ that include the effect of the QPN [47]. Additionally, to estimate $\mathcal{N}_{\text{true}}$ and, therefore, to quantify $\mathcal{B}$, we perform numerical simulations. To this end, we consider zero noise amplitude, equivalent to $r \to \infty$, a sampling rate $100\gamma_0$,
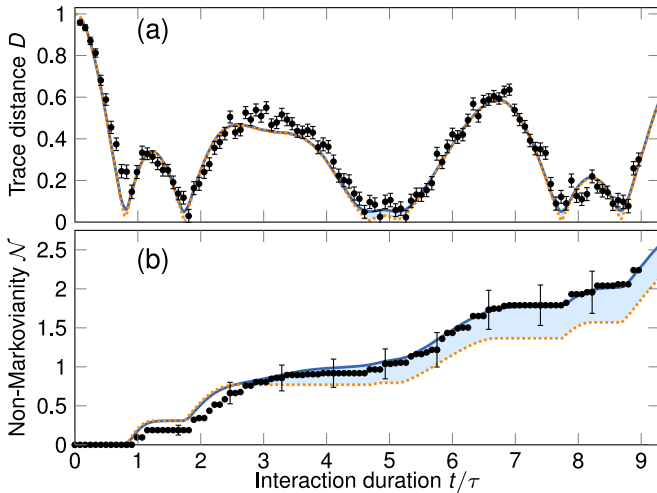
FIG. 2. Features of non-Markovianity. Experimental results (data points) for $D(t)$ and $\mathcal{N}$, for $\bar{n} = 1.0(1)$ and $\omega_z \approx \omega_E$, compared to D_{sim} and $\mathcal{N}_{\mathrm{sim}}$ (the solid lines), and D_{true} and $\mathcal{N}_{\mathrm{true}}$ (the dotted lines). The shaded areas show the effect of the fundamental quantum projection noise QPN. (a) Non-Markovian behavior is indicated by increases in D. Systematic deviations of data points [error bars: 1 standard deviation (s.d.)] from $\mathcal{N}_{\mathrm{sim}}$ reveal technical imperfections, whereas systematic deviations due to the QPN remain negligible. (b) Memory effects are evidenced by increasing $\mathcal{N}$. Noise yields an increasing bias, predominantly, when amplitudes in the dynamics become comparable to the QPN amplitudes. Error bars (1 s.d.) depict correlated statistical uncertainties, and we show representatives only [47].
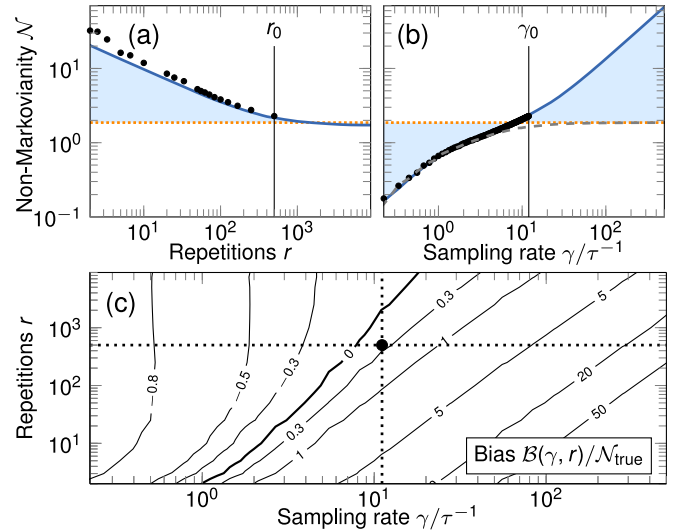

FIG. 3. Characterizing the bias $\mathcal{B}(\gamma, r)$ for parameters as in Fig. 2 and $t_{\mathrm{max}} = 9\tau$. (a) and (b) Experimental results $\mathcal{N}(\gamma, r)$ (data points), compared to $\mathcal{N}_{\mathrm{sim}}$ (the solid lines) and $\mathcal{N}_{\mathrm{true}}$ (the dotted lines), highlight $\mathcal{B}(\gamma, r)$ (the shaded area); error bars omitted for clarity. (a) We find that $\mathcal{B}(\gamma_0, r_0)/\mathcal{N}_{\mathrm{true}} \approx +17\%$ and it substantially increases for $r < r_0$ due to the QPN. The bias approaches negative values for $r > r_0$, indicating that amplitudes of fast dynamics in D are missed by our choice of γ_0. (b) The QPN leads to $\lim_{\gamma \to \infty} \mathcal{B}(\gamma, r_0) \to \infty$, whereas finite sampling yields negative $\mathcal{B}$ for $\gamma\tau < 8$. The dashed line illustrates $\lim_{r \to \infty} \mathcal{N}(\gamma, r)$. (c) The relative bias $\mathcal{B}(\gamma, r)/\mathcal{N}_{\mathrm{true}}$ reveals the nontrivial impact of the QPN and sampling on the measurement of $\mathcal{N}$. The dot marks our choice of (γ_0, r_0), and the dotted lines correspond to cuts depicted in (a) and (b).

and all other parameters fixed according to the experimental realizations [47].

First, we consider an example to discuss features of recorded non-Markovian behavior. In Fig. 2, we show measured D and $\mathcal{N}$ (data points) for $\bar{n} = 1.0(1)$ and resonant interaction $\omega_z/\omega_E = 1.000(2)$ and find good agreement with numerical simulations (the solid lines). Error bars depict the amount of QPN, whereas additional experimental uncertainties are neglected. Information, initially encoded in S, is transferred to E or S-E correlations, evidenced by decreasing D and flat $\mathcal{N}$. Memory effects are witnessed whenever D increases, accounted for by an increase in $\mathcal{N}$. The estimated true numerical results (the dotted lines) deviate from data in D only for particular durations, indicating residual systematic or technical effects. In contrast, they increasingly deviate from data in $\mathcal{N}$. We find that the QPN accumulates a systematic bias in $\mathcal{N}$. Predominantly, the increases in $\mathcal{B}$ occur for durations of near constant $\mathcal{N}$. Here, amplitudes of the dynamical evolution of D become comparable to noise amplitudes in D that are a direct consequence of the QPN.

Next, we present results to investigate $\mathcal{N}(\gamma, r)$ for $t_{\mathrm{max}} = 9\tau$. In Figs. 3(a) and 3(b), we quantify the impact of the QPN on $\mathcal{N}$ as a function of r and γ for the evolution depicted in Fig. 2. We vary r for fixed $\gamma = \gamma_0$ by postselection of random subensembles of the r_0 experimental realizations, generate resampled evolutions $D(t)$, and evaluate $\mathcal{N}(\gamma_0, r)$ [47]. The results, depicted in Fig. 3(a), agree with corresponding simulations. For increasing r, the results approach the estimated $\mathcal{N}_{\mathrm{true}}$.

However, for $r \gg r_0$, we find a significant underestimation. To explain this, we vary the mean sampling rate by random postselection of data points for $r = r_0$ [47] and show $\mathcal{N}(\gamma, r_0)$ in Fig. 3(b). When sampling rates are too low, fast dynamical features in D are missed, and $\mathcal{B} < 0$ as noted above. However, sampling rates that approach reasonable values overestimate $\mathcal{N}_{\mathrm{true}}$ due to the contribution of the QPN. Figure 3(c) summarizes our findings and illustrates the significant variation of $\mathcal{B}(\gamma, r)/\mathcal{N}_{\mathrm{true}}$ and its divergence for increasing γ for practical (finite) r.

Despite the presence of this bias, we demonstrate in the following local quantum probing [2] and evaluate the significance of our results in a system where this remains feasible by numerical simulations. Based on these results, we propose that our system can provide a reference for more complex studies of non-Markovian dynamics. To this end, we present two paradigmatic examples, where S probes the coupling to and properties of E. In a first measurement series, we probe changes in S-E couplings by variation of ω_z near ω_E for $\bar{n} = 0.09(2)$ and determine $\mathcal{N}(\gamma_0, r_0)$. Figure 4(a) depicts $\mathcal{N}(\gamma_0, r_0, \omega_z)$ for three distinct $t_{\mathrm{max}} = \{2, 5, 9\}\tau$'s. We observe resonances near $\omega_z \approx \omega_E$ that differ significantly in shape, depending on t_{max}. For small t_{max}, recorded $\mathcal{N}$'s feature a double-peak structure. This reflects an expected increase in the effective coupling rate Ω' (faster dynamics) for a detuning from resonance by $\delta\omega_z \equiv \omega_z - \omega_E$, which can be estimated by $\Omega' \propto \sqrt{\Omega^2 + \delta\omega_z^2}$. In contrast, for larger t_{max}, line shapes become
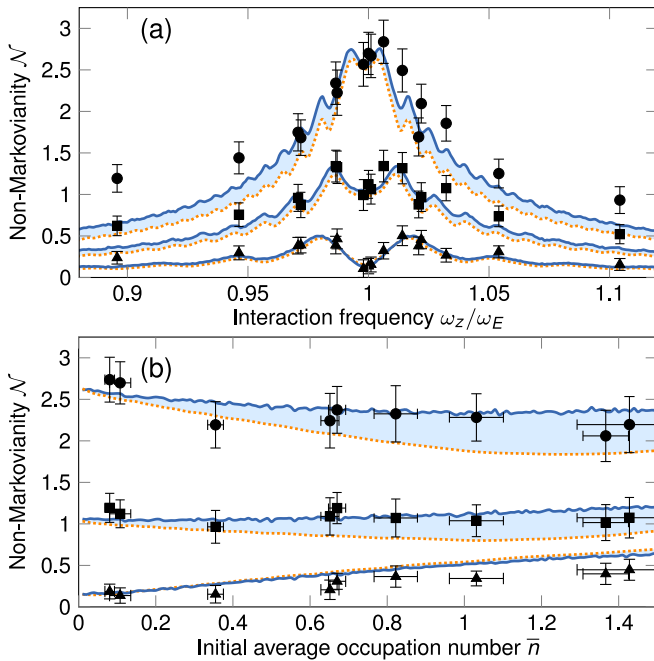
FIG. 4. Application of local quantum probing. Experimental results (data points, error bars: 1 s.d.) of $\mathcal{N}(\gamma_0, r_0)$ for $t_{max} = \{2, 5, 9\}\tau$'s (the triangles, squares, and circles), compared to corresponding (the solid lines) and true (the dotted lines) numerical results. (a) We choose $\bar{n} = 0.09(2)$ to ensure elementary quantum dynamics. In turn, $D(t)$'s are close to trivial, i.e., sinusoidal with variable frequencies and amplitudes. We observe a distinct resonance signal near $\omega_z \approx \omega_E$, and different t_{max}'s give insight on the time scales of information flow. Contributions of the QPN (the shaded areas) are near constant. (b) We observe positive and negative slopes in $\mathcal{N}(\bar{n})$ for $\omega_z/\omega_E = 1.000(2)$, reflecting increasingly complex S-E dynamics. Here, the bias varies with $\bar{n}$ and t_{max} and significantly hampers the detection of predicted features.

dominated by the resonant S-E interaction since amplitudes in $D(t)$ are $\propto \Omega^2/\Omega'^2$, i.e., they are largest for $\omega_z = \omega_E$, cf. [47]. Comparing our data to $\mathcal{N}_{sim}$ and $\mathcal{N}_{true}$, we estimate $\mathcal{B}/\mathcal{N}_{true} \approx 18\%$ on average with small variations, and we can experimentally resolve predicted features. In a second series of measurements, we probe the environmental state by tuning the initial $\bar{n}$. In Fig. 4(b), we depict experimental and numerical results of $\mathcal{N}(\gamma_0, r_0, \bar{n})$ for $t_{max} = \{2, 5, 9\}\tau$'s and $\omega_z \approx \omega_E$ and compare them to $\mathcal{N}_{true}$. For short durations, we find an increase in $\mathcal{N}(\bar{n})$, whereas for longer durations true values suggest a decrease in $\mathcal{N}(\bar{n})$. We reveal that $|\mathcal{B}/\mathcal{N}_{true}|$ varies substantially between 0% and 45%, depending on t_{max} and $\bar{n}$. For increasing $\bar{n}$, the spin interacts with a larger number of Fock states, and $D(t)$ features a less trivial frequency spectrum [47]. This results in a faster and more complex dynamics $D(t)$ that cannot be resolved with constant significance for fixed γ_0 and r_0.

Generally, recording $\mathcal{N}(\gamma, t_{max})$ can enable observations of environmental properties on time scales set by γ and t_{max}. Finding relevant parameter regimes for specific quantum probing applications is a multidimensional problem that increases with increasingly complex environments and interactions, in particular, when the system becomes intractable by numerical simulations. In the case of detection of strong

or robust variations in $\mathcal{N}$, the systematic bias may be less detrimental. However, we anticipate strategies to still estimate $\mathcal{B}$ and $\mathcal{N}$ if an increased accuracy is required. For example, it can be possible to extrapolate $\mathcal{N}(\gamma, r)$ to $r \to \infty$ guided by mathematical considerations. Furthermore, an estimation of $\mathcal{B}$ can be achieved by optimizing semiempirical models that, in turn, are tested to describe recorded $\mathcal{N}(\gamma, r)$ [47] and benchmarked in our experimental platform. Moreover, applying filters or regularization methods [51] or fitting Fourier series to recorded $D(t)$ can allow for isolating relevant dynamics from noise.

To summarize, we set up our trapped-ion system to implement an effective spin representing an open system, which we couple to an environment composed of a bosonic degree of freedom. We investigate the evolution of the trace distance of two initially orthogonal spin states to study the features of quantum memory effects. Our results demonstrate that inherent fluctuations, arising from random projection during the measurement process, yield not only uncertainties, but also a significant bias in the quantification of such effects. This affects any experimental platform and even numerical approaches, such as Monte Carlo simulations. We quantify this bias in our system to determine accurate values of the quantum NM measure. On this basis, we employ the open system as a local quantum probe to explore characteristics of system-environment couplings and environments. Our experimental platform is ideal to tune to more complex environments and couplings [37], which includes adding spin or bosonic degrees of freedom, preparing a variety of initial environmental states, and engineering couplings to additional, even classical, surroundings. It can act as a reference platform studying the intricate relations among non-Markovian dynamics, fundamental fluctuations, and time scales in, and beyond, numerically tractable regimes. Thereby, our approach can aid the understanding of physical systems in which parameters are less controlled, and other noise sources contribute substantially to an excess bias.

Furthermore, our findings imply questions concerning generalizations and applications of NM. The effect of the QPN on other measures, which are based on, e.g., the divisibility of the dynamical map [5,6,8] or the mutual information between the open system and an ancilla system [7], needs to be studied as we expect them to be significantly influenced by the QPN as well. Thus, envisioned applications of current NM measures are fundamentally limited. Consequently, it is required to extend definitions of NM measures by including physical constraints and enable a comparison of different systems. Time scales and the related flow of exploitable information depend on the application. An upper limit for the sampling rate may be given, e.g., by the so-called quantum speed limit [52], which, in turn, would limit the impact of the QPN. Based on such extensions, applications for characterizing time scales and experimentally accessible complexity measures may emerge.

[1] H.-P. Breuer and F. Petruccione, *The Theory of Open Quantum Systems* (Oxford University Press, Oxford, 2002).

[2] H.-P. Breuer, E.-M. Laine, J. Piilo, and B. Vacchini, Rev. Mod. Phys. **88**, 021002 (2016).

[3] M. M. Wolf, J. Eisert, T. S. Cubitt, and J. I. Cirac, Phys. Rev. Lett. **101**, 150402 (2008).

[4] H.-P. Breuer, E.-M. Laine, and J. Piilo, Phys. Rev. Lett. **103**, 210401 (2009).

[5] Á. Rivas, S. F. Huelga, and M. B. Plenio, Phys. Rev. Lett. **105**, 050403 (2010).

[6] D. Chruściński, A. Kossakowski, and Á. Rivas, Phys. Rev. A **83**, 052128 (2011).

[7] S. Luo, S. Fu, and H. Song, Phys. Rev. A **86**, 044101 (2012).

[8] D. Chruściński and S. Maniscalco, Phys. Rev. Lett. **112**, 120404 (2014).

[9] Á. Rivas, S. F. Huelga, and M. B. Plenio, Rep. Prog. Phys. **77**, 094001 (2014).

[10] I. de Vega and D. Alonso, Rev. Mod. Phys. **89**, 015001 (2017).

[11] T. J. G. Apollaro, C. Di Franco, F. Plastina, and M. Paternostro, Phys. Rev. A **83**, 032103 (2011).

[12] P. Haikka, S. McEndoo, G. De Chiara, G. M. Palma, and S. Maniscalco, Phys. Rev. A **84**, 031602 (2011).

[13] P. Haikka, J. Goold, S. McEndoo, F. Plastina, and S. Maniscalco, Phys. Rev. A **85**, 060101 (2012).

[14] S. Gröblacher, A. Trubarov, N. Prigge, G. D. Cole, M. Aspelmeyer, and J. Eisert, Nat. Commun. **6**, 7606 (2015).

[15] M. Žnidarič, C. Pineda, and I. García-Mata, Phys. Rev. Lett. **107**, 080404 (2011).

[16] C. Pineda, T. Gorin, D. Davalos, D. A. Wisniacki, and I. García-Mata, Phys. Rev. A **93**, 022117 (2016).

[17] K. H. Madsen, S. Ates, T. Lund-Hansen, A. Löffler, S. Reitzenstein, A. Forchel, and P. Lodahl, Phys. Rev. Lett. **106**, 233601 (2011).

[18] P. Rebentrost and A. Aspuru-Guzik, J. Chem. Phys. **134**, 101103 (2011).

[19] A. W. Chin, S. F. Huelga, and M. B. Plenio, Phys. Rev. Lett. **109**, 233601 (2012).

[20] S. Lorenzo, F. Lombardo, F. Ciccarello, and G. M. Palma, Sci. Rep. **7**, 42729 (2017).

[21] M. Gessner, M. Ramm, H. Häffner, A. Buchleitner, and H.-P. Breuer, Europhys. Lett. **107**, 40005 (2014).

[22] M. A. Nielsen and I. L. Chuang, *Quantum Computation and Quantum Information* (Cambridge University Press, Cambridge, U.K., 2000).

[23] B.-H. Liu, L. Li, Y.-F. Huang, C.-F. Li, G.-C. Guo, E.-M. Laine, H.-P. Breuer, and J. Piilo, Nat. Phys. **7**, 931 (2011).

[24] C.-F. Li, J.-S. Tang, Y.-L. Li, and G.-C. Guo, Phys. Rev. A **83**, 064102 (2011).

[25] A. Smirne, D. Brivio, S. Cialdi, B. Vacchini, and M. G. A. Paris, Phys. Rev. A **84**, 032112 (2011).

[26] S. Cialdi, A. Smirne, M. G. A. Paris, S. Olivares, and B. Vacchini, Phys. Rev. A **90**, 050301 (2014).

[27] N. K. Bernardes, A. Cuevas, A. Orieux, C. H. Monken, P. Mataloni, F. Sciarrino, and M. F. Santos, Sci. Rep. **5**, 17520 (2015).

[28] J.-S. Tang, Y.-T. Wang, G. Chen, Y. Zou, C.-F. Li, G.-C. Guo, Y. Yu, M.-F. Li, G.-W. Zha, H.-Q. Ni, Z.-C. Niu, M. Gessner, and H.-P. Breuer, Optica **2**, 1014 (2015).

[29] J. Sun, Y.-N. Sun, C.-F. Li, G.-C. Guo, K. Luoma, and J. Piilo, Sci. Bull. **61**, 1031 (2016).

[30] N. K. Bernardes, J. P. S. Peterson, R. S. Sarthour, A. M. Souza, C. H. Monken, I. Roditi, I. S. Oliveira, and M. F. Santos, Sci. Rep. **6**, 33945 (2016).

[31] M. Gessner, M. Ramm, T. Pruttivarasin, A. Buchleitner, H.-P. Breuer, and H. Häffner, Nat. Phys. **10**, 105 (2014).

[32] D. J. Wineland, Rev. Mod. Phys. **85**, 1103 (2013).

[33] D. Leibfried, R. Blatt, C. Monroe, and D. J. Wineland, Rev. Mod. Phys. **75**, 281 (2003).

[34] R. Blatt and D. Wineland, Nature (London) **453**, 1008 (2008).

[35] D. Porras, F. Marquardt, J. von Delft, and J. I. Cirac, Phys. Rev. A **78**, 010101 (2008).

[36] C. Schneider, D. Porras, and T. Schaetz, Rep. Prog. Phys. **75**, 024401 (2012).

[37] G. Clos, D. Porras, U. Warring, and T. Schaetz, Phys. Rev. Lett. **117**, 170401 (2016).

[38] C. J. Ballance, V. M. Schäfer, J. P. Home, D. J. Szwer, S. C. Webster, D. T. C. Allcock, N. M. Linke, T. P. Harty, D. P. L. Aude Craik, D. N. Stacey, A. M. Steane, and D. M. Lucas, Nature (London) **528**, 384 (2015).

[39] D. Kienzler, H.-Y. Lo, B. Keitch, L. de Clercq, F. Leupold, F. Lindenfelser, M. Marinelli, V. Negnevitsky, and J. P. Home, Science **347**, 53 (2015).

[40] T. P. Harty, D. T. C. Allcock, C. J. Ballance, L. Guidoni, H. A. Janacek, N. M. Linke, D. N. Stacey, and D. M. Lucas, Phys. Rev. Lett. **113**, 220501 (2014).

[41] J. T. Barreiro, M. Müller, P. Schindler, D. Nigg, T. Monz, M. Chwalla, M. Hennrich, C. F. Roos, P. Zoller, and R. Blatt, Nature (London) **470**, 486 (2011).

[42] C. Monroe and J. Kim, Science **339**, 1164 (2013).

[43] M. Ramm, T. Pruttivarasin, and H. Häffner, New J. Phys. **16**, 063062 (2014).

[44] M. Mielenz, H. Kalis, M. Wittemer, F. Hakelberg, U. Warring, R. Schmied, M. Blain, P. Maunz, D. L. Moehring, D. Leibfried, and T. Schaetz, Nat. Commun. **7**, 11839 (2016).

[45] N. G. van Kampen, *Stochastic Processes in Physics and Chemistry* (North Holland, Amsterdam, 1992).

[46] W. M. Itano, J. C. Bergquist, J. J. Bollinger, J. M. Gilligan, D. J. Heinzen, F. L. Moore, M. G. Raizen, and D. J. Wineland, Phys. Rev. A **47**, 3554 (1993).

[47] See Supplemental Material at http://link.aps.org/supplemental/10.1103/PhysRevA.97.020102 for further details, which includes Refs. [48–50].

[48] G. Clos, M. Enderlein, U. Warring, T. Schaetz, and D. Leibfried, Phys. Rev. Lett. **112**, 113003 (2014).

[49] T. Schaetz, A. Friedenauer, H. Schmitz, L. Petersen, and S. Kahra, J. Mod. Opt. **54**, 2317 (2007).

[50] D. J. Wineland, C. Monroe, W. M. Itano, D. Leibfried, B. E. King, and D. M. Meekhof, J. Res. Natl. Inst. Stand. Technol. **103**, 259 (1998).

[51] W. H. Press, S. A. Teukolsky, W. T. Vetterling, and B. P. Flannery, *Numerical Recipes: The Art of Scientific Computing*, 3rd ed. (Cambridge University Press, New York, 2007).

[52] S. Deffner and E. Lutz, Phys. Rev. Lett. **111**, 010402 (2013).